Acta Crystallographica Section D
Biological Crystallography
ISSN 0907-4449

Enzymes for carbon sequestration: neutron crystallographic studies of carbonic anhydrase

S. Z. Fisher,[a]* A. Y. Kovalevsky,[a] J. Domsic,[b] M. Mustyakimov,[a] D. N. Silverman,[c] R. McKenna[b] and P. Langan[a]

[a]Bioscience Division, Los Alamos National Laboratory, Los Alamos, NM 87545, USA, [b]Department of Biochemistry and Molecular Biology, PO Box 100245, University of Florida, Gainesville, FL 32610, USA, and [c]Department of Pharmacology and Therapeutics, PO Box 100267, University of Florida, Gainesville, FL 32610, USA

Correspondence e-mail: zfisher@lanl.gov

Received 12 March 2010
Accepted 25 May 2010

Carbonic anhydrase (CA) is a ubiquitous metalloenzyme that catalyzes the reversible hydration of CO_2 to form HCO_3^- and H^+ using a Zn–hydroxide mechanism. The first part of catalysis involves CO_2 hydration, while the second part deals with removing the excess proton that is formed during the first step. Proton transfer (PT) is thought to occur through a well ordered hydrogen-bonded network of waters that stretches from the metal center of CA to an internal proton shuttle, His64. These waters are oriented and ordered through a series of hydrogen-bonding interactions to hydrophilic residues that line the active site of CA. Neutron studies were conducted on wild-type human CA isoform II (HCA II) in order to better understand the nature and the orientation of the Zn-bound solvent (ZS), the charged state and conformation of His64, the hydrogen-bonding patterns and orientations of the water molecules that mediate PT and the ionization of hydrophilic residues in the active site that interact with the water network. Several interesting and unexpected features in the active site were observed which have implications for how PT proceeds in CA.

1. Introduction

Carbonic anhydrases (CAs) are ubiquitous enzymes that are found in diverse organisms from humans to archaebacteria. There is considerable interest in using CA as a biological carbon-sequestration agent owing to the reaction that it catalyzes. It is also plausible to use CA in algal cultures to produce HCO_3^- from dissolved CO_2 and make uptake of HCO_3^- more efficient (Bao & Trachtenberg, 2006; Trachtenberg *et al.*, 2003).

Human carbonic anhydrase II (HCA II) is an ∼29 kDa cytosolic protein that is predominantly found in red blood cells, where it uses a Zn–hydroxide mechanism to catalyze the reversible hydration of CO_2 to form HCO_3^- and H^+. The HCO_3^- produced is readily displaced by a water molecule, zinc solvent (ZS), that has to be activated to an OH^- *via* a proton-transfer step to regenerate the active site for the next round of catalysis (Silverman & Lindskog, 1988; Christianson & Fierke, 1996). A recent structure of HCA II in complex with CO_2 revealed the details of substrate binding and conversion; however, the details of the subsequent proton transfer are less clear (Domsic *et al.*, 2008). The proton-transfer step is hypothesized to proceed through a hydrogen-bonded network of water molecules that spans the distance between the active-site Zn and an internal proton-shuttling residue, His64. The exact mechanism is not clear and there are many possibilities, including a Grotthuss-type concerted H^+ hopping through hydrogen-bonded water chains or movement through a series

of Zundel ($H_5O_2^+$) and/or Eigen ($H_9O_5^+$) cations (De Grotthuss, 1806). A variety of plausible pathways out of the HCA II active site have been suggested (Silverman & McKenna, 2007; Maupin *et al.*, 2009).

There are several hydrophilic residues that line the active site and are involved in hydrogen bonds to the ordered water network, namely Tyr7, Asn62, Asn67, Thr199 and Thr200. The positions of the water molecules in this network appear to be very conserved and persist over a broad pH range. Mutagenesis of these hydrophilic active-site residues showed that the disruption of these water positions causes changes in the measured rate of proton transfer while having no effect on CO_2-hydration kinetics (Fisher *et al.*, 2007). Despite the availability of several high-resolution (to ∼1 Å) X-ray crystal structures of HCA II, there is little to no direct information on the protonation states of the active-site residues, the hydrogen bonding between the water network and HCA II, the nature of ZS in the absence of substrate and the charged state of His64. In order to address these issues, a neutron structure of H/D-exchanged HCA II was determined. Neutrons diffract strongly from both H and D atoms, making it easy to visualize and assign H/D-atom positions in neutron crystal structures. Replacing H with D atoms leads to a significant increase in signal to noise as D has a large positive scattering length (6.7 fm compared with −3.7 fm for H) and a small incoherent cross-section. Owing to these differences, neutron diffraction methods on H/D-exchanged samples can provide unique and novel information regarding the orientation and hydrogen-bonding interactions of solvent and the protonation states of amino-acid residues in proteins. A room-temperature X-ray data set was also collected from an equivalent crystal to enable a joint X-ray and neutron structure refinement. This approach significantly improves the quality of the neutron maps (Adams *et al.*, 2009).

Several interesting and novel features were observed in the neutron structure of HCA II: the side chain of His64 is exclusively in the inward conformation and neutral, the ZS appears to be an H_2O and not an OH^- as expected, the orientation and interactions of solvent in the active site are clearly visible and Tyr7 is observed to be unprotonated. The importance of these observations and how they pertain to proton transfer is discussed. This is the first report of a neutron structure of carbonic anhydrase.

2. Materials and methods

Wild-type human carbonic anhydrase II was expressed, purified and crystallized as described elsewhere (Fisher *et al.*, 2009). A large single crystal of HCA II (1.2 mm^3) was grown using a nine-well glass-plate setup in a sandwich box (Hampton Research). The conditions and procedure have been described in detail elsewhere (Fisher *et al.*, 2010). The crystal was subject to vapor H/D exchange by introducing perdeuterated precipitant liquid plugs on either side of the mounted crystal. Neutron and X-ray data collection were conducted as described in detail elsewhere (Fisher *et al.*, 2009).

Time-of-flight (TOF) Laue neutron diffraction data were collected at the Protein Crystallography Station using a wavelength range of 0.6–7.0 Å and the crystal diffracted neutrons to 2.0 Å resolution. A total of 41 settings were collected with 32 h exposure time for each frame. The data set was 84.6% complete, with a mean $I/\sigma(I)$ of 3.8 and an $R_{\rm p.i.m.}$ of 17.1 overall. Room-temperature X-ray data were collected in-house using a Rigaku R-AXIS IV^{++} detector and a 1.54 Å

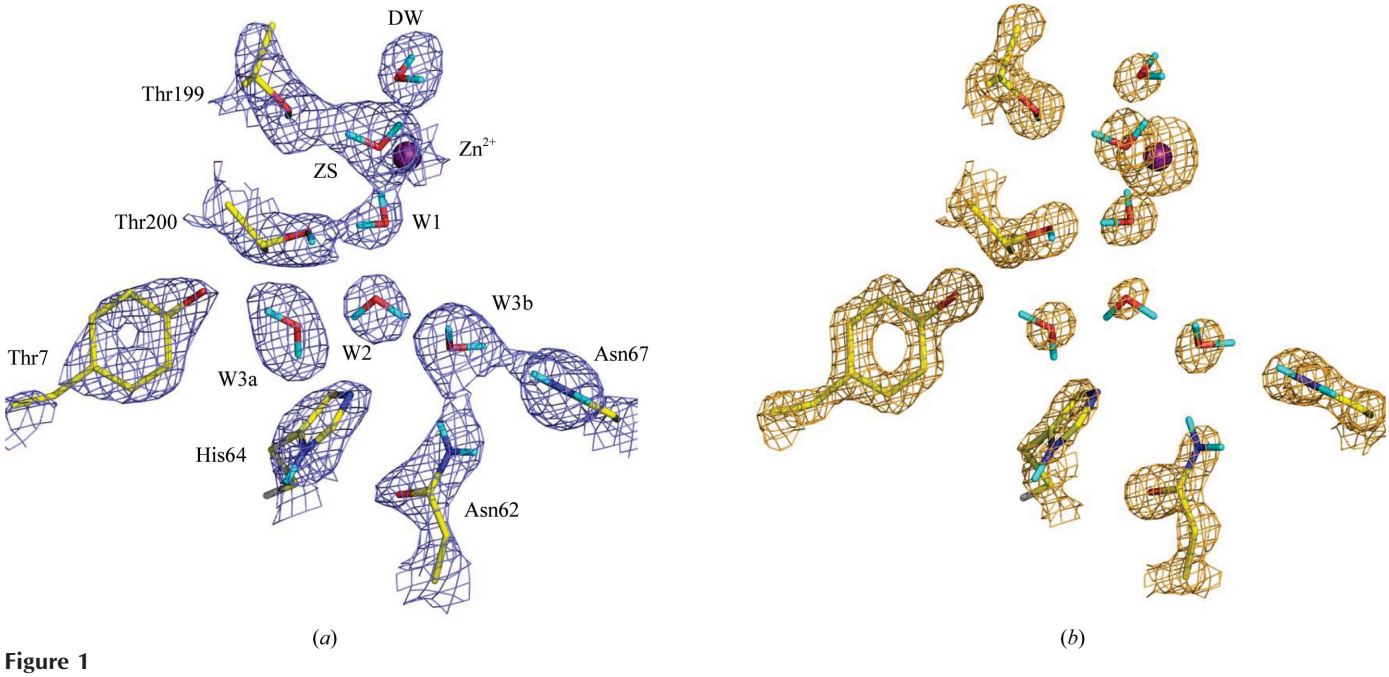

Figure 1
The active site of wild-type HCA II. (*a*) The $2F_o - F_c$ nuclear density map of the active site is shown in blue and is contoured at 1.5σ; (*b*) the $2F_o - F_c$ electron-density map is shown in orange and is contoured at 2.5σ. Active-site residues and solvent are shown in ball-and-stick representation and are labeled. D atoms are shown in cyan.

Cu $K\alpha$ rotating-anode generator. A total of 1255 settings with 2 min exposures each were collected to 1.5 Å resolution. The data set was 95.9% complete with a mean $I/\sigma(I)$ of 31.0 and an R_{merge} of 5.8 overall. The crystal belonged to space group $P2_1$, with unit-cell parameters a = 42.6, b = 41.6, c = 72.8 Å, β = 104.6°. Neutron data were processed with a version of *d*TREK* modified for TOF data analysis (Langan & Greene, 2004) and wavelength-normalized with *LAUENORM* (Helliwell *et al.*, 1989). X-ray data were indexed and reduced with *HKL*-2000 (Otwinowski & Minor, 1997). Initial model refinement started with just the X-ray data in *SHELXL* until the *R* factors converged (Sheldrick, 2008). At this point H and D atoms were included in the model and the refinement was moved to *nCNS* (Adams *et al.*, 2009), a modified version of *CNS* (Brünger *et al.*, 1998) that allows simultaneous refinement of a model against both neutron and X-ray diffraction data sets. The details of the refinement procedure are discussed elsewhere (Fisher *et al.*, 2009). The final model had R_{cryst}/R_{free} factors of 27.5/28.6 and 16.1/17.3 for the neutron and X-ray data, respectively. The model contained 4072 protein atoms (including H and D) and 232 D_2O molecules. The average *B* factors for the main chain, side chains and solvent were 21.5, 24.2 and 38.7 Å^2, respectively. The model had good standard geometry, with r.m.s.d. bond lengths and angles of 0.01 Å and 1.793°, respectively. The final model and experimental neutron data have been deposited in the Protein Data Bank with PDB code 3kkx (Fisher *et al.*, 2010).

3. Results and discussion

3.1. The nature of the Zn-bound solvent

The network of solvent that stretches from the Zn center to the proton shuttle, His64, consists of several well ordered waters, designated DW, ZS, W1, W2, W3a and W3b (Figs. 1 and 2). The unique information from the neutron structure is the position of the D atoms of these waters and, by implication, the hydrogen bonds that they participate in. From the nuclear maps we can clearly see the nature of the Zn-bound solvent (ZS) and it appears as D_2O. This is the first direct evidence of the nature of ZS. Even in atomic resolution X-ray crystal structures it is not possible to distinguish between Zn—OH^- and Zn—H_2O based on metal–O distances; the distances can range from 1.98–2.11 Å for either and neutron diffraction may be the only way to distinguish between them (Orpen *et al.*, 1989). The presence of a D_2O at the Zn is unexpected, however, owing to the high pH of crystallization (>9). The pK_a of ZS is well established as ∼7 and it is reasonable to expect an OH^- bound in the crystal (Silverman & Lindskog, 1988). It may be that the combined effect of H/D exchange and the interactions and surroundings of ZS contribute to a much higher than expected pK_a for ZS.

3.2. Water network

DW is the solvent molecule that is displaced upon substrate binding and its two D atoms point into the large hydrophobic pocket that is devoid of other water molecules (Domsic *et al.*, 2008). ZS is involved in two very short hydrogen bonds to DW and W1, with an average O···O distance of 2.5 Å. ZS and W1 act as hydrogen-bond donors to Thr199 and Thr200, respectively (Fig. 2). A surprising observation was that the two O atoms of W1 and W2 are pointing towards each other (Figs. 1 and 2). W2 is a hydrogen-bond donor to both W3a and W3b and this means that there is no continuous hydrogen-bonded chain connecting ZS to His64. There would have to be a rearrangement in this configuration during catalysis to allow transfer of a proton along this path. The electron-density map is shown for comparison in Fig. 1 and it is clear that the nuclear maps show more details of the hydrogen bonding and D-atom positions than are attainable with the X-ray structure alone.

3.3. Conformation and neutral state of His64

The proton-shuttling residue His64 has previously been observed to occupy two conformations in many different X-ray crystal structures that have been termed the inward and outward positions (Nair & Christianson, 1991; Fisher *et al.*, 2005). In the current neutron structure His64 is only observed in the inward conformation and is uncharged/neutral (Fig. 2). The unprotonated imidazole NE2 is pointing towards the active site and solvent waters W2, W3a and W3b but does not engage in hydrogen bonds with these waters. The N···O distances between the imidazole NE2 and the waters range from 3.5 to 4.6 Å. There is considerable room around this residue and it is reasonable to expect a rotation along χ_1 and/or χ_2 that will place it closer to the waters during catalysis. For example, a −30° rotation along χ_1 will place NE2 between 2.3 and 3.3 Å away from these waters.

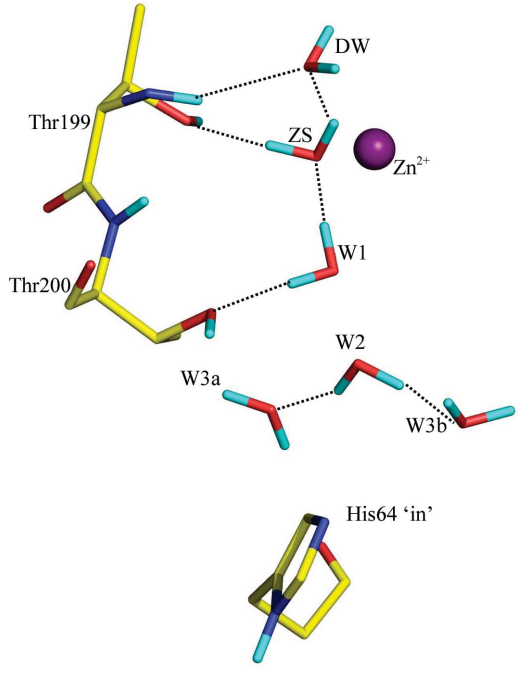

Figure 2
Details of solvent and hydrogen bonds in the active site. Hydrogen bonds are shown as dashed lines and O···D distances are indicated. Active-site residues and water molecules are shown in ball-and-stick representation and are labeled. D atoms are shown in cyan.

3.4. Tyr7 appears deprotonated

An unexpected observation was that the phenolic O of Tyr7 appears not to be protonated (Figs. 3*a* and 3*b*). No H or D atom is observed from inspection of positive and negative $2F_o - F_c$ nuclear maps (Fig. 3*b*). There are several plausible reasons for this, including incomplete H/D exchange at this atomic position, flexibility/disorder of this residue or its deprotonation owing to the high pH of crystallization. However, the most likely explanation is the high pH because there is no evidence of H being present in negative nuclear maps and Tyr7 has a low average *B* factor (∼20 Å^2 compared with an overall average of 22 Å^2 for the whole protein) and does not appear to be disordered. Lowered pK_a values for Tyr residues in the range 7–9 have been reported and these usually occur owing to proximity to positively charged species such as Lys or Arg or metals. In HCA II Tyr7 is ∼7 Å away from the Zn^{2+} and it is not clear whether this is close enough to have an effect (Jeans *et al.*, 2002; Pival *et al.*, 2008). The functional significance of a deprotonated Tyr7 in the active site is uncertain. However, it is known that CA can support PT at high pH and if this residue is deprotonated it could have a profound effect on how PT proceeds under high-pH conditions. The presence of such a negative species could assist in the stabilization of an excess of H^+. A low-pH neutron structure of wild-type HCA II would reveal the charge states of Tyr7 and His64 and could provide additional information on how the hydrogen-bonding patterns change in response to changes in charge.

3.5. Proposed proton-transfer pathway based on neutron structure

The unique information obtained from the neutron structure of HCA II suggests a pathway for proton transfer during the catalyzed hydration (Fig. 2). Owing to the discontinuous hydrogen bonding in the water network there has to be a rearrangement of the hydrogen bonds to 'open' the pathway. A possibility is the breakage of the ZS–DW and ZS–W1 bonds and flipping of the waters to establish hydrogen bonds between ZS and W1 and between W1 and W2. When the ZS deprotonates to form the catalytically active Zn—OH^-, the excess H^+ can move down the chain and take the form of a hydrated H^+ in the form of a Zundel cation ($H_5O_2^+$) between W1 and W2 or an Eigen cation ($H_9O_4^+$) with W2 as H_3O^+ and W1, W3a and W3b involved in stabilizing it. These events would be the same whether the PT mechanism was concerted or stepwise. After this, a slight rotation of uncharged His64 would place it in a perfect position to accept the excess H^+, becoming charged and flipping to the outward conformation to deliver the H^+ to bulk solvent or buffer.

3.6. Backbone H/D exchange of amide groups

Refinement of the occupancy of the D atoms found on the backbone amide groups makes it possible to map the extent of H/D exchange (Fig. 4). Fig. 4(*a*) shows a ribbon diagram of the HCA II neutron structure with the *B* factors of the C^α atoms plotted in a rainbow representation (with blue to red representing the lowest to the highest *B* factor). It is clear from this diagram that the core β-sheet is very well ordered and that the highest thermal fluctuations occur in the surface-coil and helical regions. The level of exchange has been categorized into three groups for the purposes of discussion and these are shown in Fig. 4(*b*) (blue, not exchanged; green, partially exchanged; red, completely exchanged): D occupancies of 0.00–0.29 are considered to be not exchanged (*i.e.* all or mostly H), those of 0.30–0.59 are partially H/D exchanged and those over 0.60 are considered to be completely exchanged (*i.e.* all or mostly D). Overall, ∼34% of all backbone amides are completely exchanged to D and a further ∼30% are partially exchanged; 36% are considered to be not exchanged. It should be pointed out that there is no correlation between hydrogen-bond length (and, by inference, strength) and the level of H/D exchange. This was clearly illustrated in the study by Bennett *et al.* (2008). It appears that solvent accessibility plays a dominant role in the level of H/D exchange. Also, Fig. 4 illustrates the strong correlation between the thermal *B* factors and the level of backbone amide H/D exchange. This is especially clear in the central β-sheet (blue in both panels of Fig. 4) that forms the core of the enzyme and supports the active-site residues. However, there are a few areas that at first glance appear to be counterintuitive (arrows in Fig. 4*b*). These surface coiled elements did not undergo significant H/D exchange and yet they have some of the higher *B* factors when inspected in Fig. 4(*a*). This is because the loop backbone amides are hydrogen bonded to each other, effectively shielding them from H/D exchange, while the side chains of these regions are completely exchanged and are involved in crystal-packing interactions. Fig. 5 shows a per-residue comparison between the *B* factors and

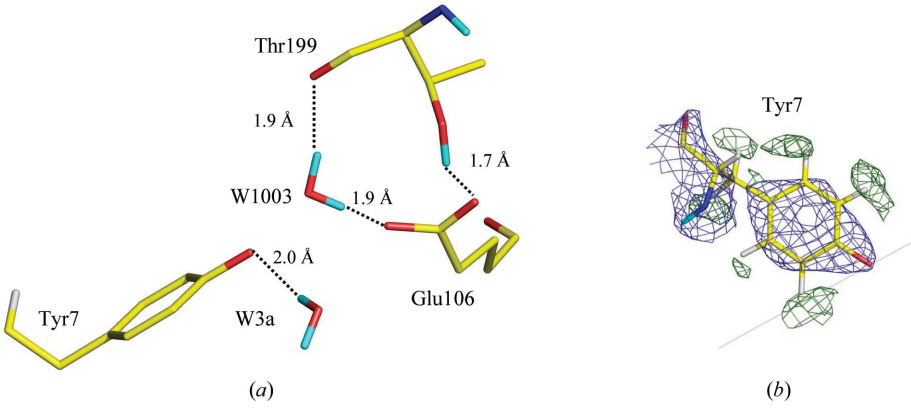

Figure 3
Tyr7 interactions and charged state. (*a*) Tyr7 is deprotonated and forms a hydrogen bond (dashed lines) to W3a. (*b*) $2F_o - F_c$ positive and negative nuclear density maps reveal H atoms but no H or D atom on the phenolic O atom of Tyr7. Active-site residues and water molecules are labeled and are shown in ball-and-stick representation; D atoms are shown in cyan.

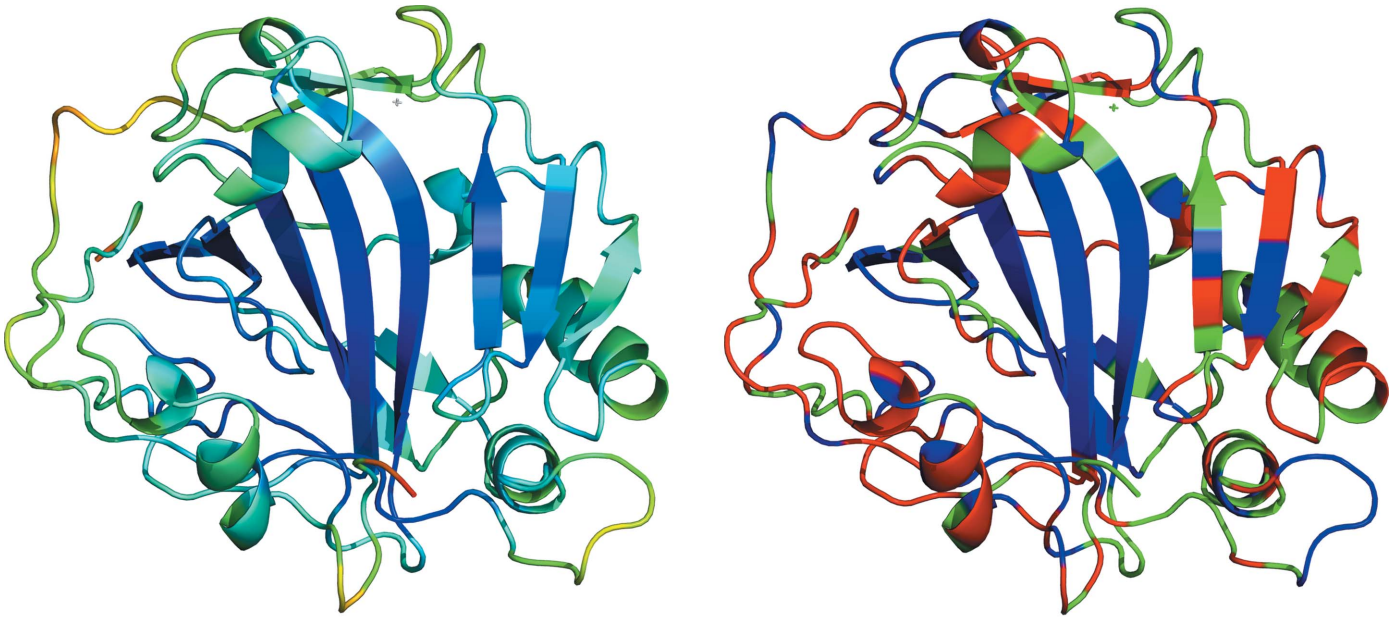

Figure 4
Ribbon diagram of HCA II showing *B* factors and the level of H/D exchange of backbone amides. (*a*) *B* factors of C^{α} atoms; the rainbow indicates lowest (blue) to highest (red) *B* factors. (*b*) Level of H/D exchange of backbone amides: blue, not exchanged (all H); green, partially exchanged (partially D); red, completely exchanged (all D).

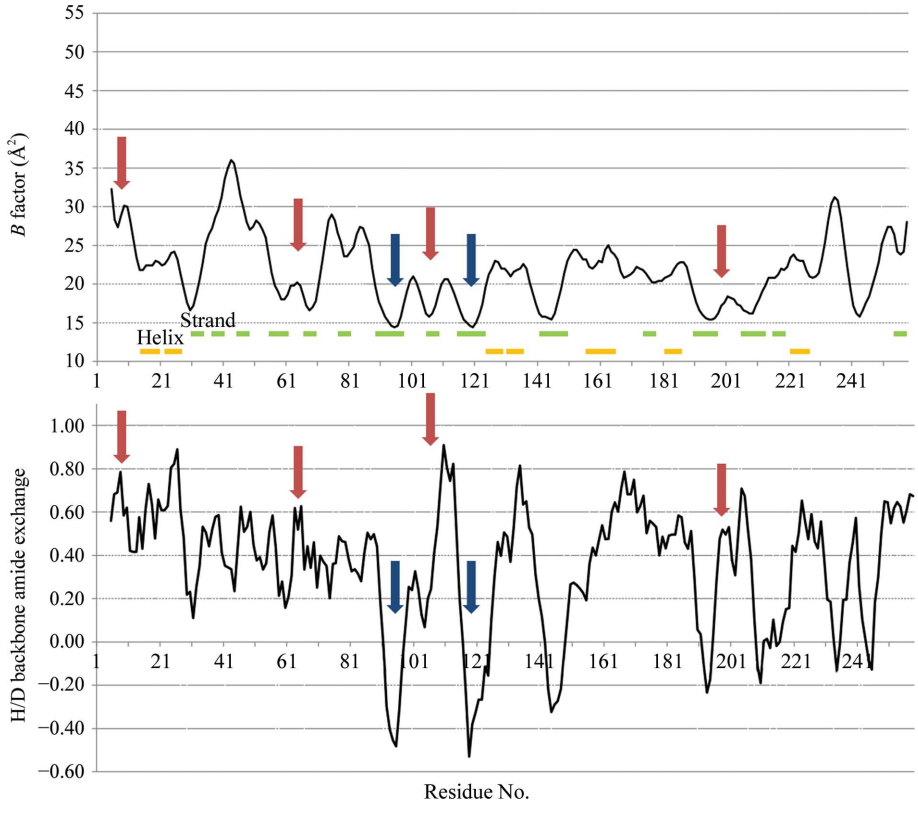

Figure 5
Plots illustrating the *B* factors and level of H/D backbone amide exchange per residue. Data are represented as a five-point moving average; helical regions are indicated as yellow bars and β-strand regions are indicated as green bars. The red arrows show hydrophilic active-site residues (Tyr7, Ans62, His64, Asn67, Glu106, Thr199 and Thr200) that interact with the water network; the blue arrows show the positions of the Zn ligands (His94, His96 and His199).

backbone amide exchange. The helical and strand regions are also indicated and this supports what is visually obvious in Fig. 4: that the strand regions have the lowest *B* factors and undergo the lowest amount of H/D exchange. This is in contrast to the fully H/D-exchanged active-site residues that sit on this scaffold and point towards the solvent-filled active site (red arrows). The Zn ligands, His94, His86 and His119, are found in areas in which the least amount of backbone H/D exchange occurs (blue arrows). However, even though the backbone is shielded, the Zn-ligand side chains are all exchanged, probably owing to their proximity to D_2O in the active site.

To determine whether H/D exchange affects the overall fold or geometry of the molecule, the structures of hydrogenous (all H), fully perdeuterated (all D) and H/D-exchanged (both H and/or D) protein were superimposed and compared. This analysis yielded an r.m.s.d. for all atoms of less than 0.2 Å; thus, the structures are completely isomorphous and there are no differences between them.

Being able to map the level and extent of H/D exchange gives a snapshot of solvent accessibility as well as

of thermally fluctuating regions in the protein. Neutron data are unique in that they provide both kinds of information from the same data. This could be very useful for identifying target residues from highly exchanged regions for rational mutagenesis to create enzymes with increased thermostability.

4. Conclusions

The neutron structure of HCA II reveals novel active-site features that have never been directly observed. The side chain of His64 is in the inward conformation only and is neutral, with the uncharged imidazole N pointing towards the active site. The D atoms of the water network that extends from the metal center to His64 are clearly visible and there is no continuous hydrogen-bonded chain, *i.e.* W1 and W2 are not optimally arranged for proton transfer. This implies that there would have to be a rearrangement during catalysis to make proton transfer possible *via* this network. Also, the Zn-bound solvent is a D_2O molecule and engages in strong hydrogen bonds to DW and W1. This is unexpected owing to the known pK_a of 7.0 for this water and the high pH of crystallization. ZS as a water must be strongly favored or stabilized in some way, probably through hydrogen-bonding interactions with DW and Thr199, to resist deprotonation at the high pH of crystallization.

The PCS is funded by the Office of Biological and Environmental Research of the Department of Energy. MM and PL were partly supported by an NIH–NIGMS-funded consortium (1R01GM071939-01) between LANL and LNBL to develop computational tools for neutron protein crystallography. AYK was supported by LDRD grant No. 20080789PRD3. This work was also partially funded by grants from the National Institutes of Health (GM25154; DNS and RM) and the Thomas Maren Foundation (RM).

References

Adams, P. D., Mustyakimov, M., Afonine, P. V. & Langan, P. (2009). *Acta Cryst.* D**65**, 567–573.
Bao, L. & Trachtenberg, M. C. (2006). *J. Membr. Sci.* **280**, 330–334.
Bennett, B. C., Gardberg, A. S., Blair, M. D. & Dealwis, C. G. (2008). *Acta Cryst.* D**64**, 764–783.
Brünger, A. T., Adams, P. D., Clore, G. M., DeLano, W. L., Gros, P., Grosse-Kunstleve, R. W., Jiang, J.-S., Kuszewski, J., Nilges, M., Pannu, N. S., Read, R. J., Rice, L. M., Simonson, T. & Warren, G. L. (1998). *Acta Cryst.* D**54**, 905–921.
Christianson, D. W. & Fierke, C. A. (1996). *Acc. Chem. Res.* **29**, 331–339.
De Grotthuss, C. J. T. (1806). *Ann. Chimie (Paris)*, **58**, 54–73.
Domsic, J. F., Avvaru, B. S., Kim, C. U., Gruner, S. M., Agbandje-McKenna, M., Silverman, D. N. & McKenna, R. (2008). *J. Biol. Chem.* **283**, 30766–30771.
Fisher, S. Z., Hernandez-Prada, J., Tu, C. K., Duda, D., Yoshioka, C., An, H., Govindasamy, L., Silverman, D. N. & McKenna, R. (2005). *Biochemistry*, **44**, 1097–1105.
Fisher, S. Z., Kovalevsky, A., Domsic, J., Mustyakimov, M., McKenna, R., Silverman, D. N. & Langan, P. (2010). *Biochemistry*, **49**, 415–421.
Fisher, S. Z., Kovalevsky, A. Y., Domsic, J. F., Mustyakimov, M., Silverman, D. N., McKenna, R. & Langan, P. (2009). *Acta Cryst.* F**65**, 495–498.
Fisher, S. Z., Tu, C. K., Bhatt, D., Govindasamy, L., Agbandje-McKenna, M., McKenna, R. & Silverman, D. N. (2007). *Biochemistry*, **46**, 3803–3813.
Helliwell, J. R., Habash, J., Cruickshank, D. W. J., Harding, M. M., Greenhough, T. J., Campbell, J. W., Clifton, I. J., Elder, M., Machin, P. A., Papiz, M. Z. & Zurek, S. (1989). *J. Appl. Cryst.* **22**, 483–497.
Jeans, C., Schilstra, M. J., Ray, N., Husain, S., Minagawa, J., Nugent, J. H. A. & Klug, D. R. (2002). *Biochemistry*, **41**, 15754–15761.
Langan, P. & Greene, G. (2004). *J. Appl. Cryst.* **37**, 253–257.
Maupin, C. M., McKenna, R., Silverman, D. N. & Voth, G. A. (2009). *J. Am. Chem. Soc.* **131**, 7598–7608.
Nair, S. K. & Christianson, D. W. (1991). *J. Am. Chem. Soc.* **113**, 9455–9458.
Orpen, A. G., Brammer, L., Allen, F. H., Kennard, O., Watson, D. G. & Taylor, R. (1989). *J. Chem. Soc. Dalton Trans.*, pp. S1–S83.
Otwinowski, Z. & Minor, W. (1997). *Methods Enzymol.* **276**, 307–326.
Pival, S. L., Klimacek, M., Kratzer, R. & Nidetzky, B. (2008). *FEBS Lett.* **582**, 4095–4099.
Sheldrick, G. M. (2008). *Acta Cryst.* A**64**, 112–122.
Silverman, D. N. & Lindskog, S. (1988). *Acc. Chem. Res.* **21**, 30–36.
Silverman, D. N. & McKenna, R. (2007). *Acc. Chem. Res.* **40**, 669–675.
Trachtenberg, M. C., Cowan, R. M., Goldman, S. L., Ge, J.-J., Qin, Y.-J. & McGregor, M. L. (2003). *Proceedings of the 33rd International Conference on Environmental Systems.* Warrendale: Society of Automotive Engineers. doi:10.4271/2003-01-2499.